


Crystal structures and X-ray powder diffraction data for $AAlGe_2O_6$ synthetic leucite analogs ($A = K, Rb, Cs$)

Anthony M. T. Bell ^{a)}

Materials and Engineering Research Institute, Sheffield Hallam University, Sheffield S1 1WB, UK

(Received 19 February 2024; accepted 5 May 2024)

Leucites are tetrahedrally coordinated silicate framework structures with some of the silicon framework cations that are partially replaced by divalent or trivalent cations. These structures have general formulae $A_2BSi_5O_{12}$ and $ACSi_2O_6$, where A is a monovalent alkali metal cation, B is a divalent cation, and C is a trivalent cation. There are also leucite analogs with analogous tetrahedrally coordinated **germanate** framework structures. These have general formulae $A_2BGe_5O_{12}$ and $ACGe_2O_6$. In this paper, the Rietveld refinements of three synthetic Ge-leucite analogs with stoichiometries of $AAlGe_2O_6$ ($A = K, Rb, Cs$) are discussed. $KAlGe_2O_6$ is $I4_1/a$ tetragonal and is isostructural with $KAlSi_2O_6$. $RbAlGe_2O_6$ and $CsAlGe_2O_6$ are $I\bar{4}3d$ cubic and are isostructural with $KBSi_2O_6$.

© The Author(s), 2024. Published by Cambridge University Press on behalf of International Centre for Diffraction Data. This is an Open Access article, distributed under the terms of the Creative Commons Attribution licence (<http://creativecommons.org/licenses/by/4.0/>), which permits unrestricted re-use, distribution and reproduction, provided the original article is properly cited.

[doi:10.1017/S088571562400023X]

Keywords: powder diffraction, Rietveld refinement, leucite minerals, germanate framework structures

I. INTRODUCTION

Synthetic anhydrous analogs of the silicate framework minerals such as leucite ($KAlSi_2O_6$) and pollucite ($CsAlSi_2O_6$) can be prepared with the general formulae $A_2BSi_5O_{12}$ and $ACSi_2O_6$, where A is a monovalent alkali metal cation, B is a divalent cation, and C is a trivalent cation. These structures have the same topology, with B and C cations partially substituting onto tetrahedrally coordinated sites (T-sites) in the silicate framework, and charge-balancing A cations sitting in extraframework channels. The A cations can be replaced by ion exchange, and Cs-containing silicate framework minerals are of potential technological interest as storage media for radioactive Cs from nuclear waste (Gatta et al., 2008, 2009).

Many ambient temperature leucite analogs are known with different crystal structures and different A , B , and C cations (Bell, 2024). These structures all have the same topology, $CsAlSi_2O_6$ is $Ia\bar{3}d$ cubic (Beger, 1969), $KBSi_2O_6$ is $I43d$ cubic (Millini et al., 1993), and $KAlSi_2O_6$ is $I4_1/a$ tetragonal (Mazzi et al., 1976). All these high symmetry structures have *disordered* T-site cations. However, lower symmetry structures are also known with *ordered* T-site cations. Examples of these cation-ordered structures are Eu^{2+} -doped $CsZnSi_2O_6$ (Hariyani et al., 2020, $Pa\bar{3}$ cubic), $Cs_2CdSi_5O_{12}$ (Bell et al., 1994b, $Pbca$ orthorhombic), and $K_2MgSi_5O_{12}$ (Bell et al., 1994a, $P2_1/c$ monoclinic).

However, it is also possible to synthesize analogs of leucite and pollucite in which silicon is replaced with germanium. These Ge-leucites have **germanate** framework structures with the same topology as the leucite structure. In these cases,

$A_2BGe_5O_{12}$ and $ACGe_2O_6$ leucite analogs can be synthesized where B and C cations partially substitute onto tetrahedrally coordinated sites (T-sites) in the **germanate** framework, and charge-balancing A cations sit in extraframework channels.

Lattice parameters have been reported for $A_2BGe_5O_{12}$ analogs ($A = Rb, Cs$; $B = Be, Mg, Zn, Co, Fe, Ni, Cu, Cd$) (Richerson and Hummel, 1972; Torres-Martinez et al., 1984; Torres-Martinez and West, 1989). Lattice parameters have also been reported for analogs $ACGe_2O_6$ ($A = K, Rb, Cs, NH_4$; $C = B, Al, Ga, Cr, Fe$) (Torres-Martinez et al., 1984; Torres-Martinez and West, 1989). Additionally, lattice parameters have been reported for $K_{0.8}Rb_{0.2}AlGe_2O_6$ (Klaska, 1978).

This paper reports the Rietveld refinements (Rietveld, 1969) of three Ge-leucites with stoichiometries of $AAlGe_2O_6$ ($A = K, Rb, Cs$). A crystal structure has been reported for $CsAlGe_2O_6$ (Tripathi and Parise, 2002), but no crystal structures have yet been reported for the K and Rb analogs. Powder Diffraction File (Gates-Rector and Blanton, 2019) data have been reported for these three Ge-leucite analogs. The PDF numbers are 00-37-1349 ($KAlGe_2O_6$), 00-37-348 ($RbAlGe_2O_6$), 00-37-347, and 04-012-2039 ($CsAlGe_2O_6$).

II. EXPERIMENTAL

A. Sample synthesis

All three samples were prepared from appropriate stoichiometric mixtures of K_2CO_3 , Rb_2CO_3 , $Cs_2CO_3 \cdot 3H_2O$, GeO_2 , and Al_2O_3 . These mixtures were loaded into Pt crucibles and heated in air in a furnace. For all three samples, the mixtures were heated for 12 h at 1073 K (to decompose carbonates). For $A = K$, the crucible was air quenched, but for

^{a)} Author to whom correspondence should be addressed. Electronic mail: anthony.bell@shu.ac.uk



A = Rb and Cs the crucibles were quenched by dipping the bottom of the crucible in the bucket of cold water. For A = K, the mixture was then heated for 3 days at 1373 K. The sample was then removed from the furnace, reground, and then reheated for 4 days at 1373 K. For A = Rb, the mixture was then reground before further heating for 4 days at 1373 K. For A = Cs, the mixture was then reground before further heating for 50 h at 1373 K. The sample was then ground again before heating for 1 more day at 1373 K.

B. X-ray powder diffraction data collection

After heating, the samples were removed from the Pt crucibles, ground with a mortar and pestle, and then mounted on low-background silicon wafers with a drop of acetone prior to ambient temperature X-ray powder diffraction.

For A = K, data were collected on a PANalytical X'Pert Pro MPD using Cu $K\alpha$ X-rays, with a nickel β -filter and a $3.3473^\circ 2\theta$ wide 255 channel PIXCEL-1D area detector. Data were collected in two scans using Data Collector 5.5a (PANalytical, 2017), scan 1 lasted 1 h, and scan 2 lasted 7 h and 30 min. These data were collected over the range of $5\text{--}100^\circ 2\theta$ with a step width of $0.0131^\circ 2\theta$ and an effective counting times of 118 s per point (scan 1) and 919 s per point (scan 2). For both scans, the beam size was defined with a 20 mm mask, fixed antiscatter ($1/4^\circ$), and divergence ($1/8^\circ$) slits. These two scans were summed together after data collection.

For A = Rb, data were also collected on a PANalytical X'Pert Pro MPD using Cu $K\alpha$ X-rays, with a nickel β -filter and a $3.3473^\circ 2\theta$ wide 255 channel PIXCEL-1D area detector. Data were collected in a single scan over 22 h using Data Collector 5.5a (PANalytical, 2017). These data were collected over the range of $10\text{--}100^\circ 2\theta$ with a step width of $0.0131^\circ 2\theta$ and an effective counting time of 2838 s per point. The beam size was defined with a 20 mm mask, fixed antiscatter ($1/4^\circ$), and divergence ($1/8^\circ$) slits.

For A = Cs, data were collected on a PANalytical Empyrean diffractometer using Co $K\alpha$ X-rays with an iron β -filter and a $3.3473^\circ 2\theta$ wide 255 channel PIXCEL-3D area detector. Data were collected in a single scan over 19 h using Data Collector 5.1a (PANalytical, 2014). These data were collected over the range of $15\text{--}100^\circ 2\theta$ with a step width of $0.0131^\circ 2\theta$ and an effective counting time of 2592 s per point. The beam size was defined with a 20 mm mask, fixed divergence antiscatter ($1/4^\circ$) slit, and automatic divergence slit with a 20 mm long beam footprint. These diffracted intensities were converted from an automatic divergence slit mode to a fixed divergence slit mode in HighScore Plus (PANalytical, 2009) prior to data analysis.

No smoothing or α_2 stripping was done on any of these data. Both diffractometers were calibrated with an external NIST SRM640e silicon standard.

C. X-ray powder diffraction data analysis

All powder diffraction data were analyzed using HighScore Plus and the ICDD Powder Diffraction File. For A = K, analysis of the powder diffraction data showed that this sample was mostly KAlGe_2O_6 (PDF# 00-37-1349) with GeO_2 (PDF# 00-43-1016) and KAlGeO_4 (PDF# 01-78-1173) present as minor phases. For A = Rb, analysis

of the powder diffraction data showed that this sample was mostly $\text{RbAlGe}_2\text{O}_6$ (PDF# 00-37-0348) with GeO_2 (PDF# 04-03-0650) and Al_2O_3 (PDF# 01-73-5928) present as minor phases. For A = Cs, analysis of the powder diffraction data showed that this sample was single-phase $\text{CsAlGe}_2\text{O}_6$ (PDF# 00-37-0347), apart from an unassigned Bragg reflection at about $17.8^\circ 2\theta$.

All Rietveld refinements (Rietveld, 1969) for these data were done using GSAS-II (Toby and von Dreele, 2013). Table I shows details of the refinements, including the number of observed and calculated reflections, the number of structural parameters and profile parameters, and the *R* factors.

For A = K, the crystal structure of KAlGe_2O_6 was refined using the $I4_1/a$ tetragonal structure of KAlSi_2O_6 (Mazzi et al., 1976) as a starting model. The lattice parameters from PDF# 00-37-1349 were used and Ge atoms were put on the Si sites. The crystal structures of GeO_2 (Haines et al., 2002) and KAlGeO_4 (Sun et al., 2019) were used for the minor phases. Rietveld refinement showed that for A = K, the sample consisted of 98.1(5) wt% KAlGe_2O_6 , 0.32(31) wt% GeO_2 , and 1.57(7) wt% KAlGeO_4 . In this KAlGe_2O_6 crystal structure, all atoms were located on the $I4_1/a$ 16f Wyckoff general position. There is one 16f position for K, three 16f positions for T-sites (disordered $1/3^{\text{rd}}$ Al and $2/3^{\text{rd}}$ Ge), and six 16f positions for O. The isotropic temperature factors of the T-site atoms Al and Ge were constrained to be the same on each T-site but were allowed to vary between different T-sites. All isotropic temperature factors for the six O sites were constrained to have the same value. The T–O interatomic distances were soft-constrained to be $1.74 \pm 0.02 \text{ \AA}$ (average bond distance for tetrahedral Al–O and Ge–O). This assumption is made due to complete T-site disorder ($1/3^{\text{rd}}$ Al and $2/3^{\text{rd}}$ Ge on each T-site) as it was not possible to refine chemically sensible T-site occupancies. This constraint distance was determined from the differences between the ionic radii for Si^{4+} and Ge^{4+} (Shannon, 1976) and then added the difference to the KAlSi_2O_6 T–O soft constraint distance of $1.68 \pm 0.02 \text{ \AA}$.

For A = Cs, the crystal structure of $\text{CsAlGe}_2\text{O}_6$ was refined using the $I\bar{4}3d$ cubic structure of $\text{CsAlGe}_2\text{O}_6$ (Tripathi and Parise, 2002) as a starting model. Due to the presence of the unassigned Bragg reflection at about $17.8^\circ 2\theta$, the data from 15 to $18^\circ 2\theta$ were excluded from the Rietveld refinement, which was then done assuming a single phase of $\text{CsAlGe}_2\text{O}_6$. For A = Rb, the crystal structure of $\text{CsAlGe}_2\text{O}_6$ was used as a starting model, the lattice parameters from PDF# 00-37-0348 were used, and Rb was replaced Cs in the extraframework cation site. The crystal structures of GeO_2 (Haines et al., 2002) and Al_2O_3 (Finger and Hazen, 1978) were used for the minor phases. Rietveld refinement showed that for A = Rb, the sample consisted of 88.80(24)

TABLE I. Details of Rietveld refinements.

Stoichiometry	KAlGe_2O_6	$\text{RbAlGe}_2\text{O}_6$	$\text{CsAlGe}_2\text{O}_6$
Observed reflections	97	81	47
Calculated reflections	1654	181	88
Refined parameters	61	40	35
<i>R</i> _factor	0.03171	0.02881	0.01237
<i>wR</i> _factor	0.04540	0.04605	0.02060
<i>wR</i> _expected	0.01253	0.00565	0.00800
goodness_of_fit	3.62	8.15	2.347

TABLE II. Refined lattice parameters compared with those for starting structures.

Stoichiometry	Space group	<i>a</i> (Å)	<i>b</i> (Å)	<i>c</i> (Å)	<i>V</i> (Å ³)
KAlSi ₂ O ₆ ^a	<i>I</i> 4 ₁ / <i>a</i>	13.09(1)	13.09(1)	13.75(1)	2356(4)
KAlGe ₂ O ₆ ^b	<i>I</i> 4 ₁ / <i>a</i>	13.3316(5)	13.3316(5)	14.3206(3)	2545.23(19)
CsAlGe ₂ O ₆ ^c	<i>I</i> 4̄3 <i>d</i>	13.945(2)	13.945(2)	13.945(2)	2711.8(5)
CsAlGe ₂ O ₆ ^b	<i>I</i> 4̄3 <i>d</i>	13.8951(6)	13.8951(6)	13.8951(6)	2682.8(3)
RbAlGe ₂ O ₆ ^b	<i>I</i> 4̄3 <i>d</i>	13.7153(5)	13.7153(5)	13.7153(5)	2579.97(26)

^aMazzi et al. (1976)

^bThis work.

^cTripathi and Parise (2002).

wt% RbAlGe₂O₆, 0.24(7) wt% GeO₂, and 10.96(23) wt% Al₂O₃. For both A = Cs and A = Rb, the T–O interatomic distances were also soft-constrained to be 1.74 ± 0.02 Å.

VESTA (Momma and Izumi, 2011) was used to plot crystal structures.

III. RESULTS AND DISCUSSION

Crystal structures have been refined for AAlGe₂O₆ (A = K, Rb, Cs) synthetic leucite analogs from X-ray powder diffraction data. The crystal structure of KAlGe₂O₆ is isostructural with the *I*4₁/*a* tetragonal structure of KAlSi₂O₆. The crystal structures of RbAlGe₂O₆ and CsAlGe₂O₆ are both isostructural with the *I*4̄3*d* cubic structure of CsAlGe₂O₆ (Tripathi and Parise, 2002). All refined structures have disordered T-site cations.

Table II shows the comparison of the refined lattice parameters for AAlGe₂O₆ (A = K, Rb, Cs) with the starting structures used for Rietveld refinement. Table III, Table IV, and Table V similarly show refined interatomic distances and angles. Table VI shows the tetrahedral angle variances for the T-sites (Robinson et al., 1971) in these germanate framework structures.

A. KAlGe₂O₆ structure

Figures 1 and 2, respectively, show the Rietveld difference and the VESTA crystal structure plots for the refined crystal structure of KAlGe₂O₆. Table II shows that this crystal

structure has a unit cell volume that is larger than the isostructural KAlSi₂O₆, which was used as a starting model for Rietveld refinement, reflecting the difference between the ionic radii for Si⁴⁺ and Ge⁴⁺ (Shannon, 1976).

B. RbAlGe₂O₆ structure

Figures 3 and 4, respectively, show the Rietveld difference and the VESTA crystal structure plots for the refined crystal structure of RbAlGe₂O₆. Table II shows that the crystal structure of RbGaSi₂O₆ has a smaller unit cell volume than that of CsGaSi₂O₆, which was used as a starting model for Rietveld refinement. This also reflects the difference in the ionic radii for Rb⁺ and Cs⁺ cations (Shannon, 1976).

C. CsAlGe₂O₆ structure

Figures 5 and 6, respectively, show the Rietveld difference and the VESTA crystal structure plots for the refined crystal structure of CsAlGe₂O₆. Table II shows that the crystal structure of CsAlGe₂O₆ has a slightly smaller unit cell volume than that of the CsAlGe₂O₆ structure (Tripathi and Parise, 2002), which was used as a starting model for Rietveld refinement.

D. Comparisons between AAlGe₂O₆ structures

Figures 2, 4, and 6 show plots of the AAlGe₂O₆ crystal structures. Figure 2 (A = K) shows that the central channel

TABLE III. Refined interatomic A–O distances (Å) (A = K, Rb, Cs).

K1–O1 ¹	3.088(15)	Rb1–O1 ^{1,2,3}	4.000(10)
K1–O1 ²	3.607(15)	Rb1–O1 ^{16,17,18}	3.392(9)
K1–O2 ¹	4.268(12)	Rb1–O2 ^{4,5,6}	3.084(8)
K1–O2 ¹⁴	2.974(14)	Rb1–O2 ^{16,17,18}	3.467(11)
K1–O3 ⁴	3.855(15)	Mean Rb–O	3.486(10)
K1–3 ⁸	3.062(11)	Cs1–O1 ^{1,2,3}	3.435(8)
K1–O4 ⁸	3.065(14)	Cs1–O1 ^{16,17,18}	3.862(12)
K1–O4 ¹⁴	3.784(13)	Cs1–O2 ^{4,5,6}	3.246(11)
K1–O5 ¹	2.822(11)	Cs1–O2 ^{16,17,18}	3.957(11)
K1–O5 ⁴	3.630(17)	Mean Cs–O	3.625(11)
K1–O6 ¹	3.860(14)		
K1–O6 ⁴	3.162(13)		
Mean K–O	3.431(14)		

A = K symmetry operations for O atoms in A–O

distances: ¹*x,y,z*; ²3/4 – *y*, 1/4 + *x*, 1/4 + *z*; ⁴3/4 + *y*, 3/4 – *x*, 3/4 + *z*;

⁸1/4 – *y*, 1/4 + *x*, 1/4 – *z* ¹⁴3/4 + *y*, 1/4 – *x*, 1/4 – *z*

A = Rb and Cs symmetry operations for O atoms in A–O

distances: ¹*x,y,z* ²*z,x,y* ³*y,z,x* ⁴3/4 + *y*, 1/4 – *x*, 3/4 – *z* ⁵3/4 – *z*, 3/4 + *y*, 1/4 – *x* ⁶1/4 – *x*, 3/4 – *z*, 3/4 + *y* ¹⁶3/4 + *x*, 3/4 + *z*, 3/4 + *y* ¹⁷3/4 + *y*, 3/4 + *x*, 3/4 + *z* ¹⁸3/4 + *z*, 3/4 + *y*, 3/4 + *x*

TABLE IV. Refined interatomic T–O distances (Å) (T = Al/Ge).

A = K		A = Rb	
T1–O1 ¹	1.727(5)	T1–O1 ¹	1.619(5)
T1–O1 ⁸	1.729(6)	T1–O1 ⁴⁵	1.630(5)
T1–O2 ¹	1.726(6)	T1–O2 ¹	1.776(5)
T1–O4 ²	1.699(6)	T1–O2 ⁴	1.725(6)
T2–O2 ¹	1.733(6)	Mean T–O	1.688(5)
T2–O3 ¹	1.707(6)	A = Cs	
T2–O4 ¹	1.675(6)	T1–O1 ¹	1.729(5)
T2–O5 ¹	1.776(6)	T1–O1 ⁴⁵	1.719(5)
T3–O3 ⁴	1.681(6)	T1–O2 ¹	1.716(5)
T3–O5 ¹	1.712(6)	T1–O2 ⁴	1.723(5)
T3–O6 ¹	1.702(6)	Mean T–O	1.722(5)
T3–O6 ¹⁴	1.733(6)		
Mean T–O	1.717(6)		

A = K symmetry operations for O atoms in T–O distances:
¹x,y,z; ²3/4 – y, 1/4 + x, 1/4 + z; ⁴3/4 + y, 3/4 – x, 3/4 + z;
⁸1/4 – y, 1/4 + x, 1/4 – z ¹⁴3/4 + y, 1/4 – x, 1/4 – z

A = Rb and Cs symmetry for O atom operations for T–O distances: ¹x,y,z ⁴⁵3/4 + z, 1/4 – y, 3/4 – x ⁴3/4 + y, 1/4 – x, 3/4 – z

for the $I4_1/a$ tetragonal structure shows greater framework collapse (Taylor and Henderson, 1968) compared to the corresponding channels for the $I\bar{4}3d$ cubic structures for A = Rb and Cs, reflecting the differences in the sizes of the extraframework alkali metal cations (Shannon, 1976).

Table III shows that the mean A–O distances are smallest for A = K and largest for A = Cs, also reflecting the differences

TABLE V. Refined interatomic angles (°) (T = Al/Ge).

A = K		A = Rb	
O1–T1–O1 ^{1,8}	116.2(7)	O1–T1–O1 ^{1,45}	103.3(7)
O1–T1–O2 ^{1,1}	111.8(7)	O1–T1–O2 ^{1,1}	102.6(5)
O1–T1–O2 ^{8,1}	104.0(6)	O1–T1–O2 ^{45,1}	115.7(4)
O1–T1–O4 ^{1,2}	107.8(7)	O1–T1–O2 ^{1,4}	114.7(4)
O1–T1–O4 ^{8,2}	105.7(6)	O1–T1–O2 ^{45,4}	106.7(4)
O2–T1–O4 ^{1,2}	111.2(6)	O2–T1–O2 ^{1,4}	113.6(7)
O2–T2–O3 ^{1,1}	96.0(6)	T1–O1–T1 ^{1,14}	148.6(6)
O2–T2–O4 ^{1,1}	106.6(5)	T1–O2–T1 ^{1,13}	128.6(5)
O3–T2–O4 ^{1,1}	111.9(5)	Mean O–T1–O	109.4(5)
O2–T2–O5 ^{1,1}	110.0(5)	Mean T1–O–T1	138.6(5)
O3–T2–O5 ^{1,1}	112.1(9)	A = Cs	
O4–T2–O5 ^{1,1}	117.9(8)	O1–T1–O1 ^{1,45}	129.2(6)
O3–T3–O5 ^{4,1}	118.8(7)	O1–T1–O2 ^{1,1}	113.1(6)
O3–T3–O6 ^{4,1}	113.5(5)	O1–T1–O2 ^{45,1}	109.2(5)
O5–T3–O6 ^{1,1}	108.0(6)	O1–T1–O2 ^{1,4}	102.2(5)
O3–T3–O6 ^{4,14}	99.0(6)	O1–T1–O2 ^{45,4}	106.1(6)
O5–T3–O6 ^{1,14}	117.6(6)	O2–T1–O2 ^{1,4}	88.0(8)
O6–T3–O6 ^{1,14}	98.0(7)	T1–O1–T1 ^{1,14}	128.1(7)
T2–O1–T1 ^{1,14}	139.8(6)	T1–O2–T1 ^{1,13}	141.4(7)
T1–O2–T2 ^{1,1}	150.3(7)	Mean O–T1–O	108.0(6)
T2–O3–T3 ^{1,2}	132.0(5)	Mean T1–O–T1	134.8(7)
T2–O4–T2 ^{4,1}	140.3(7)		
T2–O5–T3 ^{1,1}	124.4(4)		
T3–O6–T3 ^{1,8}	131.7(6)		
Mean O–T1–O	109.5(6)	A = Rb and Cs symmetry operations for O atoms in O–T–O angles and for T atoms in T–O–T angles:	
Mean O–T2–O	109.1(6)	¹ x,y,z; ² 3/4 – y, 1/4 + x, 1/4 + z;	
Mean O–T3–O	109.2(6)	⁴ 3/4 + y, 3/4 – x, 3/4 + z; ⁸ 1/4 – y, 1/4 + x, 1/4 – z	
Mean T–O–T	136.4(6)	¹⁴ 3/4 + y, 1/4 – x, 1/4 – z	

in the sizes of the extraframework alkali metal cations (Shannon, 1976). Table IV shows that there are some significant differences between the mean T–O distances in these crystal structures. All refinements were done assuming stoichiometries of $AAlGe_2O_6$, with Ge and Al in a 2:1 ratio. However, the presence of impurity phases in the A = K and Rb samples could mean that the Ge and Al may not be in an exact 2:1 ratio. This could change the mean size of the T-site cation and consequently change the mean T–O distances.

Table V shows the intratetrahedral (O–T–O) and intertetrahedral (T–O–T) angles for the three crystal structures. The mean O–T–O angles are close to the ideal tetrahedral angle of 109.47°, and the mean T–O–T angles for the three structures are similar. Table VI shows that the greatest tetrahedral distortion is for the A = Cs structure.

E. Future work on the $KAlGe_2O_6$ structure

The crystal structure of $KAlGe_2O_6$ is isostructural with the $I4_1/a$ tetragonal structure of $KAlSi_2O_6$ (Mazzi et al., 1976) and $KGaSi_2O_6$ (Bell and Henderson, 2020). Both $I4_1/a$ silicate structures undergo high temperature-phase transitions to $Ia\bar{3}d$ cubic structures, which was isostructural with $CsAlSi_2O_6$ (Beger, 1969). The phase transition temperatures were 943 K ($KAlSi_2O_6$, Palmer et al., 1997) and 673–970 K ($KGaSi_2O_6$, Bell and Henderson, 2020). It would be interesting to see if $KAlGe_2O_6$ would undergo a similar phase transition on heating, would there be a phase transition to an $Ia\bar{3}d$ or $I\bar{4}3d$ cubic structure?

TABLE VI. Tetrahedral angle variance [σ^2 , deg²]: $\sigma^2 = \Sigma(\theta - 109.47)^2/5$ (Robinson et al., 1971) where θ is the O–T–O tetrahedral angle.

Stoichiometry	Space group	σ^2 (T1) deg	σ^2 (T2) deg	σ^2 (T3) deg	σ^2 (T) deg ²
$KAlGe_2O_6$	$I4_1/a$	19.76	54.79	82.55	52.36 (31.47)
$RbAlGe_2O_6$	$I\bar{4}3d$				35.23
$CsAlGe_2O_6$	$I\bar{4}3d$				185.54

Mean variance and standard deviation are given for the three tetrahedral sites in the A = K $I4_1/a$ structure. Variance is given for the single tetrahedral site in the A = Rb and Cs $I\bar{4}3d$ structures.

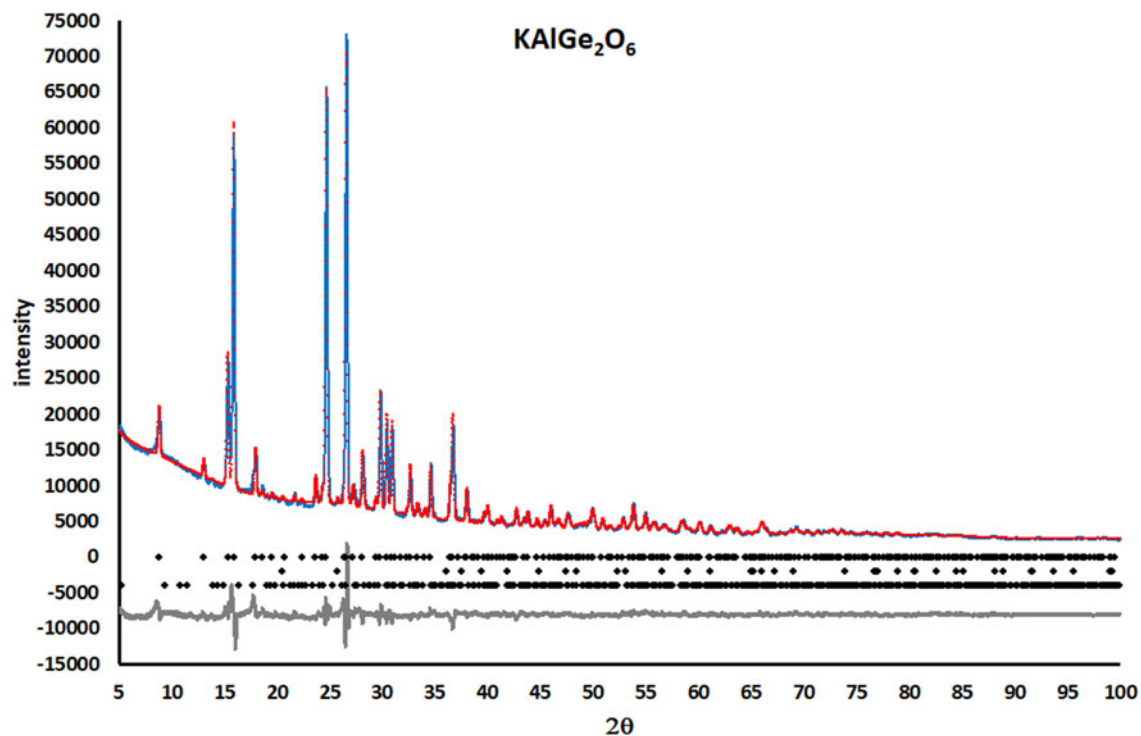


Figure 1. Rietveld difference plot for KAlGe_2O_6 . Red circles represent observed data points, blue line represents calculated data points, and the green line represents difference curves. The upper line of black crosses represents positions of Bragg reflections for KAlGe_2O_6 , the middle line of black crosses represents positions of Bragg reflections for GeO_2 , and the lower line of black crosses represents positions of Bragg reflections for KAlGeO_4 .

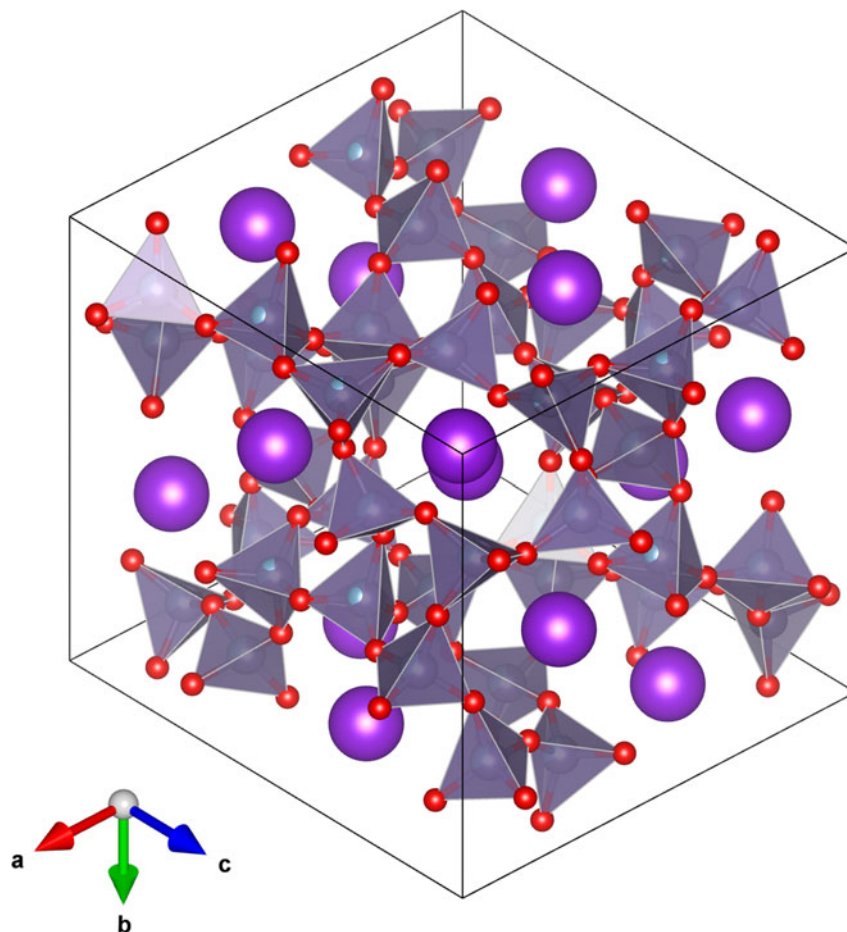


Figure 2. VESTA $I4_1/a$ tetragonal structure plot for KAlGe_2O_6 , viewed down $[1\bar{1}1]$ showing a channel for extraframework purple K^+ cations. Disordered $(\text{Al}/\text{Ge})\text{O}_4$ tetrahedra are shown in light purple, and O^{2-} anions are shown in red.

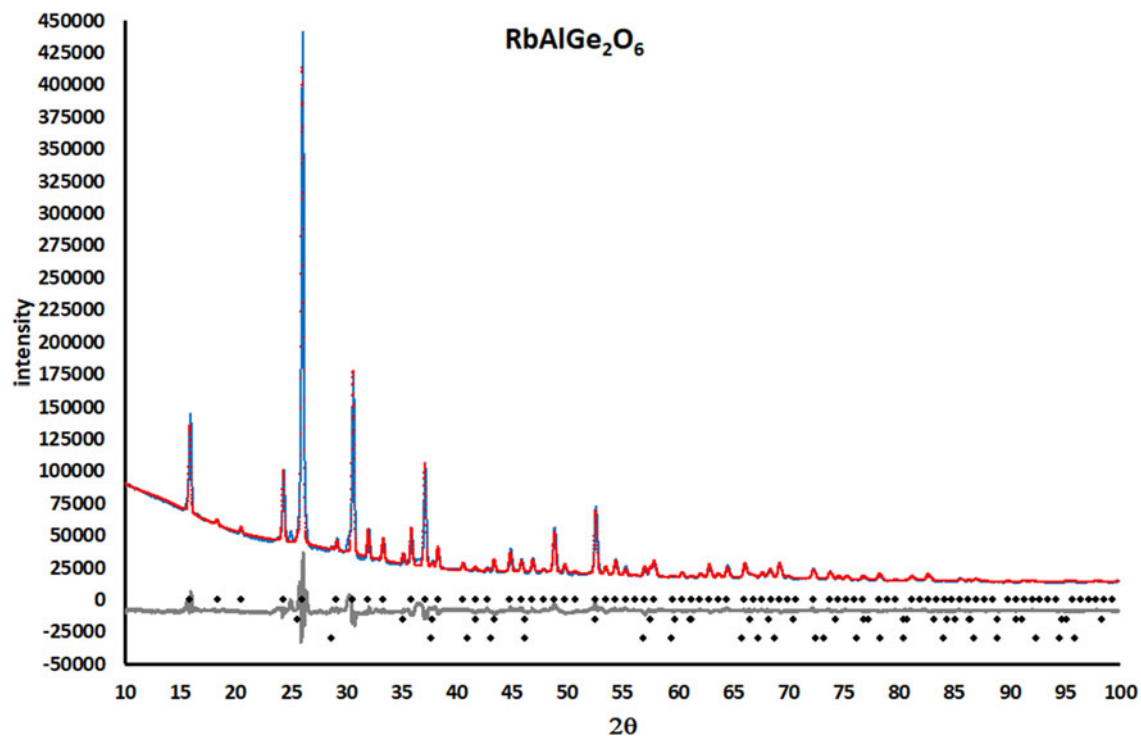


Figure 3. Rietveld difference plot for $\text{RbAlGe}_2\text{O}_6$. Red circles represent observed data points, blue line represents calculated data points, and the green line represents difference curves. The upper line of black crosses represents positions of Bragg reflections for $\text{RbAlGe}_2\text{O}_6$, the middle line of black crosses represents positions of Bragg reflections for Al_2O_3 , and the lower line of black crosses represents positions of Bragg reflections for GeO_2 .

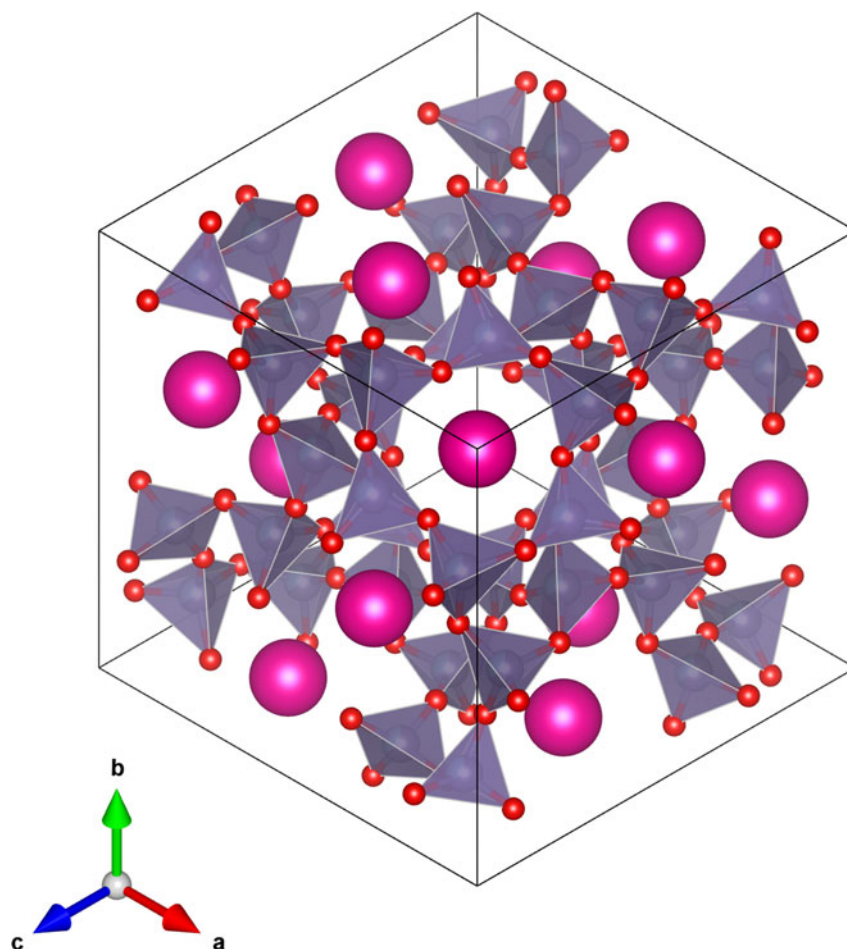


Figure 4. VESTA $I\bar{4}3d$ cubic structure plot for $\text{RbAlGe}_2\text{O}_6$, viewed down $[111]$ showing a channel for extraframework pink Rb^+ cations. Disordered $(\text{Al}/\text{Ge})\text{O}_4$ tetrahedra are shown in light purple, and O^{2-} anions are shown in red.

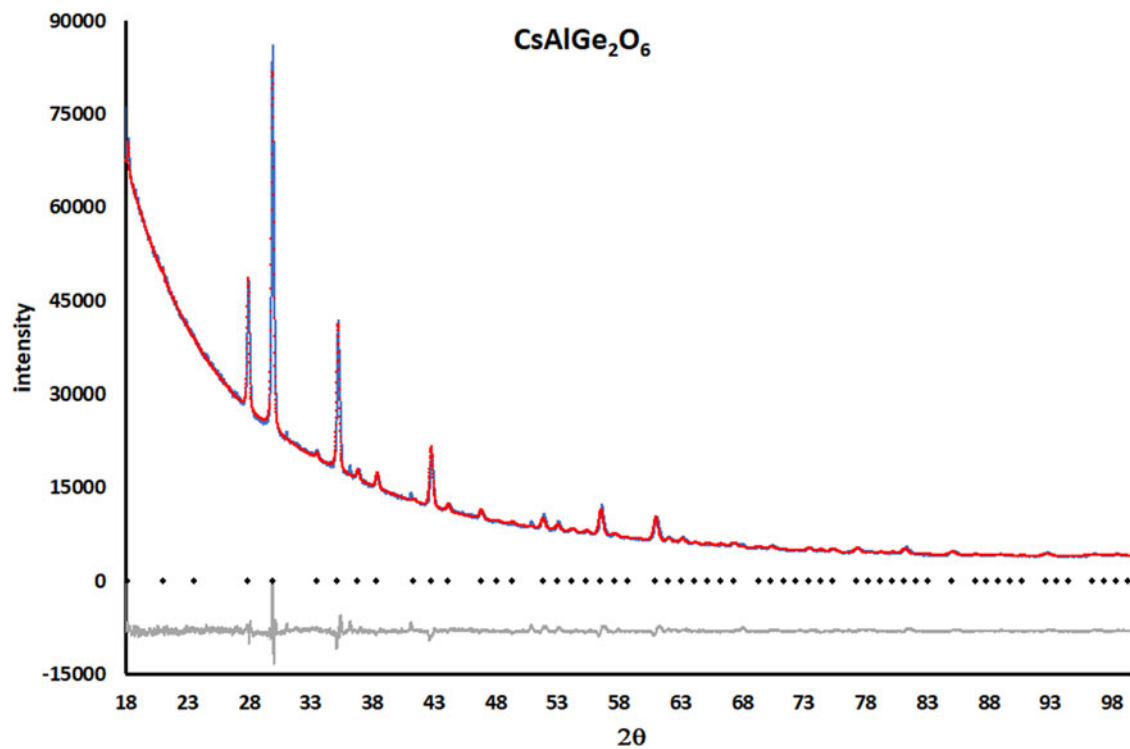


Figure 5. Rietveld difference plot for $\text{CsAlGe}_2\text{O}_6$. Red circles represent observed data points, blue line represents calculated data points, and the green line represents difference curves. The line of black crosses represents positions of Bragg reflections for $\text{CsAlGe}_2\text{O}_6$.

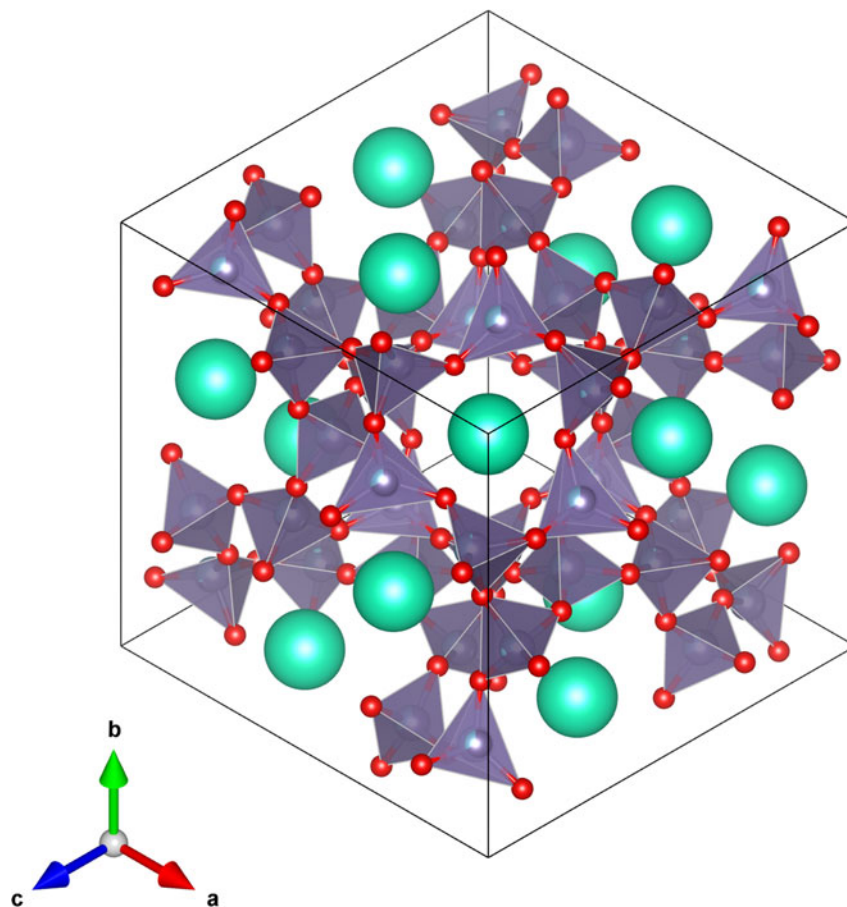


Figure 6. VESTA $I\bar{4}3d$ cubic structure plot for $\text{CsAlGe}_2\text{O}_6$, viewed down $[111]$ showing a channel for extraframework light blue Cs^+ cations. Disordered $(\text{Al}/\text{Ge})\text{O}_4$ tetrahedra are shown in light purple, and O^{2-} anions are shown in red.

IV. CONCLUSIONS

Crystal structures have been refined for $\text{AAI}\text{Ge}_2\text{O}_6$ synthetic leucite analogs ($A = \text{K}, \text{Rb}, \text{Cs}$). All refined structures have disordered T-site cations. KAlGe_2O_6 is isostructural with $I4_1/a$ tetragonal KAlSi_2O_6 leucite. However, $\text{CsAlGe}_2\text{O}_6$ has the $I\bar{4}3d$ cubic space group and is isostructural with a previously published structure for $\text{CsAlGe}_2\text{O}_6$. $\text{RbAlGe}_2\text{O}_6$ also has the $I\bar{4}3d$ cubic space group and is isostructural with $\text{CsAlGe}_2\text{O}_6$.

V. DEPOSITED DATA

CIF files with information related to crystal structure, interatomic distances and angles, and powder diffraction data for KAlGe_2O_6 , $\text{RbAlGe}_2\text{O}_6$, and $\text{CsAlGe}_2\text{O}_6$ synthetic leucite analogs were deposited with the ICDD. You may request these data from ICDD at info@icdd.com.

ACKNOWLEDGEMENTS

The author wishes to acknowledge the use of the EPSRC funded National Chemical Database Service hosted by the Royal Society of Chemistry.

REFERENCES

- Beger, R. M. 1969. "The Crystal Structure and Chemical Composition of Pollucite." *Zeitschrift für Kristallographie – Crystalline Materials* 129: 280–302. doi:10.1524/zkri.1969.129.16.280.
- Bell, A. M. T. 2024. "Crystal Structures of Leucites – Past, Present, and Future?" Submitted to Crystallography Reviews.
- Bell, A. M. T., and C. M. B. Henderson. 2020. "Tetragonal-Cubic Phase Transition in KGaSi_2O_6 Synthetic Leucite Analogue and its Probable Mechanism." *Journal of Solid State Chemistry* 284: 121142. doi:10.1016/j.jssc.2019.121142.
- Bell, A. M. T., C. M. B. Henderson, S. A. T. Redfern, R. J. Cernik, P. E. Champness, A. N. Fitch, and S. C. Kohn. 1994a. "Structures of Synthetic $\text{K}_2\text{MgSi}_5\text{O}_{12}$ Leucites by Integrated X-ray Powder Diffraction, Electron Diffraction and ^{29}Si MAS NMR Methods." *Acta Crystallographica B* 50: 31–41. doi:10.1107/S0108768193008754.
- Bell, A. M. T., S. A. T. Redfern, C. M. B. Henderson, and S. C. Kohn. 1994b. "Structural Relations and Tetrahedral Ordering Pattern of Synthetic Orthorhombic $\text{Cs}_2\text{CdSi}_5\text{O}_{12}$ Leucite: A Combined Synchrotron X-ray Powder Diffraction and Multinuclear MAS NMR Study." *Acta Crystallographica B* 50: 560–6. doi:10.1107/S0108768194003393.
- Finger, L. W., and R. M. Hazen. 1978. "Crystal Structure and Compression of Ruby to 46 kbar." *Journal of Applied Physics (Melville, NY, United States)* 49: 5823–6.
- Gates-Rector, S., and T. Blanton. 2019. "The Powder Diffraction File: A Quality Materials Characterization Database." *Powder Diffraction* 34 (4): 352–60. doi:10.1017/S0885715619000812.
- Gatta, G. D., N. Rotiroli, M. Fisch, M. Kadiyski, and T. Armbruster. 2008. "Stability at High-Pressure, Elastic Behaviour and Pressure-Induced Structural Evolution of $\text{CsAlSi}_5\text{O}_{12}$: A Potential Host for Nuclear Waste." *Physics and Chemistry of Minerals* 35: 521–33.
- Gatta, G. D., R. Rinaldi, G. J. McIntyre, G. Nénert, and F. Bellatreccia. 2009. "On the Crystal Structure and Crystal Chemistry of Pollucite, $(\text{Cs}, \text{Na})_{16}\text{Al}_{16}\text{Si}_{32}\text{O}_{96}\text{nH}_2\text{O}$: A Natural Microporous Material of Interest in

- Nuclear Technology." *American Mineralogist* 94: 1560–8. doi:10.2138/am.2009.3237.
- Haines, J., O. Cambon, E. Philippot, L. Chapon, and S. Hull. 2002. "A Neutron Diffraction Study of the Thermal Stability of the Alpha-Quartz-Type Structure in Germanium Dioxide." *Journal of Solid State Chemistry* 166: 434–41.
- Hariyani, S., E. Armijo, and J. Brgoch. 2020. "Broad Green Emission in the Leucite-Like $\text{Cs}_2\text{ZnSi}_5\text{O}_{12}:\text{Eu}^{2+}$ Phosphor." *ECS Journal of Solid State Science and Technology* 9: 016015. doi:10.1149/2.0222001JSS.
- Klaska, R. 1978. "Ein synthetischer Leucit-typ mit Ordnungstrennung." *Naturwissenschaften* 65: 592–93.
- Mazzi, F., E. Galli, and G. Gottardi. 1976. "The Crystal Structure of Tetragonal Leucite." *American Mineralogist* 61: 108–15.
- Millini, R., L. Montanari, and G. Bellussi. 1993. "Synthesis and Characterization of a Potassium Borosilicate with ANA Framework Type Structure." *Microporous Materials* 1: 9–15.
- Momma, K., and F. Izumi. 2011. "VESTA 3 for Three-Dimensional Visualization of Crystal, Volumetric and Morphology Data." *Journal of Applied Crystallography* 44: 1272–6. doi:10.1107/S0021889811038970.
- Palmer, D. C., M. T. Dove, R. M. Ibberson, and B. M. Powell. 1997. "Structural Behavior, Crystal Chemistry, and Phase Transitions in Substituted Leucite: High-Resolution Neutron Powder Diffraction Studies." *American Mineralogist* 82: 16–29.
- PANalytical. 2009. *High Score Plus 2.2e (Computer Software)*. Almelo, The Netherlands, PANalytical.
- PANalytical. 2014. *Data Collector 5.1a (Computer Software)*. Almelo, The Netherlands, PANalytical.
- PANalytical. 2017. *Data Collector 5.5a (Computer Software)*. Almelo, The Netherlands, PANalytical.
- Richerson, D. W., and F. A. Hummel. 1972. "Synthesis and Thermal Expansion of Polycrystalline Cesium Minerals." *Journal of the American Ceramic Society* 55 (5): 269–73.
- Rietveld, H. M. 1969. "A Profile Refinement Method for Nuclear and Magnetic Structures." *Journal of Applied Crystallography* 2: 65–71. doi:10.1107/S0021889869006558.
- Robinson, K., G. V. Gibbs, and P. H. Ribbe. 1971. "Quadratic Elongation: A Quantitative Measure of Distortion in Coordination Polyhedra." *Science* 172: 567–70.
- Shannon, R. D. 1976. "Revised Effective Ionic Radii and Systematic Studies of Interatomic Distances in Halides and Chalcogenides." *Acta Crystallographica Section A* 32 (5): 751–67. doi:10.1107/S0567739476001551.
- Sun, W., H. Li, B. Zheng, R. Pang, L. Jiang, S. Zhang, and C. Li. 2019. "Electronic Structure and Photoluminescence Properties of a Novel Single-Phased Color Tunable Phosphor $\text{KAlGeO}_4:\text{Bi}^{3+}, \text{Eu}^{3+}$ for WLEDs." *Journal of Alloys and Compounds* 774: 477–86.
- Taylor, D., and C. M. B. Henderson. 1968. "The Thermal Expansion of the Leucite Group of Minerals." *American Mineralogist* 53 (9-10): 1476–89.
- Toby, B. H., and R. B. Von Dreele. 2013. "GSAS-II: The Genesis of a Modern Open-Source All Purpose Crystallography Software Package." *Journal of Applied Crystallography* 46 (2): 544–9. doi:10.1107/S0021889813003531.
- Torres-Martinez, L. M., and A. R. West. 1989. "Pollucite- and Leucite-Related Phases: $\text{A}_2\text{BX}_5\text{O}_{12}$ and ACX_2O_6 ($A = \text{K}, \text{Rb}, \text{Cs}$; $B = \text{Be}, \text{Mg}, \text{Fe}, \text{Co}, \text{Ni}, \text{Cu}, \text{Zn}, \text{Cd}$; $C = \text{B}, \text{Al}, \text{Ga}, \text{Fe}, \text{Cr}$; $X = \text{Si}, \text{Ge}$)." *Zeitschrift für Anorganische und Allgemeine Chemie* 578: 223–30.
- Torres-Martinez, L. M., J. A. Gard, and A. R. West. 1984. "Synthesis and Structure of a New Family of Phases, $\text{A}_2\text{MGe}_5\text{O}_{12}$: $A = \text{Rb}, \text{Cs}$; $M = \text{Be}, \text{Mg}, \text{Co}, \text{Zn}$." *Journal of Solid State Chemistry* 53: 354–9.
- Tripathi, A., and J. B. Parise. 2002. "Hydrothermal Synthesis and Structural Characterization of the Aluminogermanate Analogues of JBW, Montessonmaite, Analcime and Paracelsian." *Microporous and Mesoporous Materials* 52: 65–78.